Electrochemical and Photoelectrochemical Investigation of Single-Crystal Anatase

L. Kavan,[†,§] M. Grätzel,*[,†] S. E. Gilbert,[†] C. Klemenz,[‡] and H. J. Scheel[‡]

Contribution from the Institute of Physical Chemistry, Swiss Federal Institute of Technology, Ecublens, CH-1015 Lausanne, Switzerland, and Cristallogenèse-IMO, Swiss Federal Institute of Technology, Ch. de Bellerive 34, CH-1007 Lausanne, Switzerland

Received December 12, 1995. Revised Manuscript Received May 6, 1996[⊗]

Abstract: Single crystals of TiO_2 anatase containing 0.22% of Al and traces of V, Zr, Nb, and La were grown by chemical transport reactions employing $TeCl_4$ as the transporting agent. Electrodes having the (101) face exposed doped by reduction with hydrogen were employed. The electrochemical and photoelectrochemical behavior of a single crystal of anatase were scrutinized for the first time. Properties were compared to those of single-crystal rutile having the (001) face exposed. Impedance analysis established that the flatband potential of anatase (101) is shifted negatively by 0.2 V with regards to that of rutile (001). Interfacial capacitance measurements under forward bias indicate smaller density of surface states on anatase. Photoelectrochemical oxidation of water occurs on both rutile and anatase with incident photon-to-current conversion efficiencies close to unity at $\lambda = 300$ nm. From the comparison of U_{fb} and E_g, it follows that anatase (101) and rutile (001) electrodes differ mainly in the position of the conduction band edge. The complete photoelectrolysis of water to H_2 and O_2 is thermodynamically possible on anatase only. Photosensitized electron injection from adsorbed *cis*-Ru[L_2(SCN)$_2$] (L = 2,2′-bipyridyl-4,4′-dicarboxylic acid) proceeds with similar efficiency on both types of electrodes. However, light-induced charge separation on the single-crystal electrodes is about three times less efficient compared with nanoscopic anatase films. Anatase (101) is strikingly more active for electrochemical insertion of Li^+ than rutile (001). The diffusion coefficients for Li^+ insertion and extraction were estimated to be 2×10^{-13} and 6×10^{-13} cm^2/s, respectively.

1. Introduction

Titanium dioxide has three common polymorphs: rutile (space group $P4_2/mnm$), brookite (*Pbca*), and anatase ($I4_1/amd$). Moreover, TiO_2 adopts five additional crystal structures: TiO_2 II ("columbite", (α-PbO_2) *Pbcn*),[1,2] TiO_2 III ("baddeleyite", $P2_1/c$),[2] TiO_2 (H) ("hollandite", $I4/m$),[3] TiO_2 (R) ("ramsdellite", *Pbnm*),[4] and TiO_2 (B) ("bronze", $C2/m$).[5] These were synthesized either by a high-pressure treatment of anatase or rutile (TiO_2 II and III) or by topotactic oxidative extraction of alkali metal from $K_{0.25}TiO_2$ (hollandite), $Li_{0.5}TiO_2$ (ramsdellite), and $K_2Ti_4O_9$ (bronze). None of these latter TiO_2 modifications occur in nature, except TiO_2 (B), which was recently found in the locality Binntal in Valais, Switzerland.[6]

Rutile is the thermodynamically most stable modification of TiO_2. It is by about 1.2−2.8 kcal/mol more stable than anatase.[7] The anatase to rutile transformation occurs in the temperature range of 700−1000 °C, depending on the crystallite size[8] and impurity content.[8,9] Further investigations are required to establish whether anatase and brookite are impurity-stabilized low-temperature phases of TiO_2. The question is whether they should, in a strict sense, be regarded as modifications of TiO_2, a situation which is similar to the SiO_2-phase tridymite.

Anatase crystals were grown previously below 750 °C by chemical transport reactions employing HCl,[10−12] HBr,[11] or CCl_4[12] as transport agents. However, the reducing atmosphere created by hydrogen halides favors the formation of lower oxides and of rutile.[13] Thermodynamic calculations[14] have shown that $TeCl_4$ is an attractive transport agent for TiO_2. The reaction involved in the transport process is schematically[14,15]

$$TiO_2(s) + TeCl_4(g) \underset{T_2}{\overset{T_1}{\rightleftharpoons}} TiCl_4(g) + TeO_2(g); \qquad T_1 > T_2 \quad (1)$$

Several other transport equilibria were also proposed for the TiO_2−$TeCl_4$ system with $TeCl_2$, Cl_2, and $TeOCl_2$ as intermediates.[16] The reaction proceeds across a temperature gradient T_1−T_2, and metastable TiO_2 crystals, i.e., anatase[15,17] or brookite,[17]

* Author to whom correspondence should be addressed.
§ On leave from the J. Heyrovsky Institute of Physical Chemistry, CZ-182 23 Prague 8, Dolejskova 3, Czech Republic.
† Institute of Physical Chemistry.
‡ Cristallogenèse-IMO.
⊗ Abstract published in *Advance ACS Abstracts,* June 15, 1996.

(1) Simons, P. Y.; Dateline, F. *Acta Crystallogr.* **1967**, *23*, 334.
(2) (a) Tang, J.; Endo, *J. Am. Ceram. Soc.* **1993**, *76*, 796. (b) Lagarec, K.; Desgreniers, S. *Solid State Commun.* **1995**, *94*, 519. (c) Sato, H.; Endo S.; Sugiyama, M.; Kikegawa, T.; Shimomura, O.; Kusaba, K. *Science* **1991**, *251*, 786. (d) Haines, J.; Léger, J. M. *Physica B*, **1993**, *192*, 233 (e) Arashi, H. *J. Phys. Chem. Solids* **1992**, *53*, 355.
(3) Latroche, M.; Brohan, R.; Marchand, R.; Tournoux, M. *J. Solid State Chem.* **1980**, *81*, 78.
(4) Akimoto, J.; Gotoh, Y.; Oosawa, Y.; Nonose, N.; Kumagai, T.; Aoki, K. *J. Solid State Chem.* **1994**, *113*, 27.
(5) Marchand, R.; Brohan, R. *Mat. Res. Bull.* **1980**, *15*, 1129.
(6) Banfield, J. F.; Veblen, D. R.; Smith, D. J. *Am. Mineral.* **1991**, *76*, 343.
(7) Fahmi, A.; Minot, C.; Silvi, B.; Causá, M. *Phys. Rev. B* **1993**, *47*, 11717.
(8) Banfield, J. F.; Bischoff, B. L.; Anderson, M. A. *Chem. Geol.* **1993**, *110*, 211.
(9) MacKenzie, K. J. D. *Trans. J. Br. Ceram. Soc.* **1975**, *74* 29.
(10) Wäsch, E. *Krist. Tech.* **1972**, *7*, 187.
(11) Izumi, F.; Kodama, H.; Ono, A. *J.Cryst. Growth* **1979**, *47*, 139.
(12) Berger, H.; Tang, H.; Lévy, F. *J. Cryst. Growth* **1993**, *130*, 108.
(13) (a) Suyama, Y.; Ito, K.; Kato, A. *J. Inorg. Nucl. Chem.* **1975**, *37*, 1883. (b) Suyama, Y.; Ohmura, K.; Kato, A. *Nippon Kagaku Kaishi* **1976**, 584. (c) Peshev, P.; Babievskaya, I. Z.; Krenev, V. A. *Mater. Res. Bull.* **1977**, *12*, 1035.
(14) Niemyski, T.; Piekarczyk, W. *J.Cryst. Growth* **1967**, *1*, 177.
(15) Davtyan, G. D. *Kristllografiya* **1976**, *21*, 869 (*Sov. Phys. Crystallogr.* **1976**, *21*, 499).
(16) (a) Schäfer, H. *Z. Anorg. Allg. Chem.* **1977**, *435*, 5. (b) Brückner, W.; Oppermann, H. *Vanadium Oxide. Darstellung, Eigenschaften und Anwendugen*, Akademie Verlag: Berlin, 1983.
(17) Razumeenko, M. V.; Grunin, V. S.; Boitsov, A. *Kristallografiya* **1981**, *26*, 650 (*Sov. Phys. Crystallogr.* **1981**, *26*, 371).

S0002-7863(95)04172-2 CCC: $12.00

deposit on the colder part of the reaction vessel (T_2). Early works on the growth of anatase or brookite came to the agreement that the appearance of these modifications is conditioned by the presence of stabilizing impurities, such as Al, Ga, In,[11] V, P, Nb, Cr,[15] Fe, and Mg.[17] However, the precise mechanism of phase stabilization by such heteroatoms remains unknown.[11]

In 1993, Lévy et al.[12] reported on the first preparation of the anatase single crystal by chemical transport reactions with NH_4-Cl or HCl. These crystals were characterized by Raman spectroscopy,[2b,12] photoluminescence,[18] electronic properties (resistivity, thermopower, and Hall effect),[19] magnetic properties (EPR and magnetic susceptibility),[20] and ESCA.[21] They had a dark blue color, and showed unusually high, metal-like conductivity at $T > 60$ K.

Photolectrochemical properties of rutile single-crystal electrodes were studied by many authors[22] since the pioneering work of Fujishima and Honda.[23] On the other hand, there are no reports on anatase single-crystal electrodes, apparently due to the lack of sufficiently large anatase crystals.[22] While numerous investigations have been carried out with anatase, in particular in the form of aqueous dispersions for photocatalytic applications, all of these were performed with polycrystalline materials. Mesoporous films are receiving special attention[24] recently. Little is known about the electrochemistry of TiO_2(B)[25,26] and almost nothing about brookite[27] and other polymorphs.

Charge transfer processes at the TiO_2/electrolyte interface are expected to be sensitive to crystal structure and morphology of the exposed lattice planes. Given the vast amount of research presently performed on TiO_2 and its wide realm of applications, an in-depth analysis of these effects is urgently warranted. A matter of contention, which might be clarified by the study of the anatase single-crystal electrode, is the electrochemical intercalation of Li^+ into TiO_2. In contrast to TiO_2 (anatase) and TiO_2 (B),[25,26] the Li^+ insertion into TiO_2 (rutile)[26−29] and presumably also to TiO_2 (brookite)[26] is mostly reported to be negligible (cf., however, ref 31 for different statements). The diffusion coefficient of Li^+ in anatase is presumably smaller than that in rutile,[32] although some authors claim the opposite,[33] and some even present data without specifying the crystalline modification of their TiO_2.[34] Disagreement exists also about the composition and structure of the product, i.e. Li_xTiO_2 (anatase). The maximum insertion ratios, x were reported to be 0.5,[26] 0.6,[28] 0.8,[29] or 1.[35] However, $Li_{0.5}TiO_2$ (anatase) is the only well-defined product of the topotactic reaction, and x values exceeding 0.5−0.7 should be taken with care.[36] Li^+ ions are assumed to occupy tetrahedral voids[37] or both tetrahedral and octahedral voids[35] in the anatase packing of oxygen atoms. A more substantiated finding is that Li^+ in $Li_{0.5}TiO_2$ is located in highly distorted octahedral interstices with a coordination number of 5; this structure may transform thermally into the isomeric spinel (superconducting at 13 K).[36]

The aim of this paper is to scrutinize the salient electrochemical and photoelectrochemical properties of n-TiO_2 (anatase). To the best of our knowledge, this is the first photoelectrochemical study of single-crystal anatase. Preliminary experiments showed the previously described highly doped anatase[12,19] to be photoinactive, presumably due to its metal-like character. Therefore, colorless and insulating anatase crystals first had to be grown, which were subsequently n-doped under controlled conditions, and used as semiconductor electrodes.

2. Experimental Section

Materials. TiO_2 (Merck, anatase powder 2 N), $TeCl_4$ (3 N, Alfa), and Al_2O_3 (4 N, Johnson-Matthey) were used as received. The starting TiO_2 powder contained the following impurities (ICP analysis, see below; in parentheses is the impurity content in wt·ppm): Al (550), Nb (260), V (250), Zr (140), La (14). *cis*-$Ru[L_2(SCN)_2]\cdot 2H_2O$, L = 2,2′-bipyridyl-4,4′-dicarboxylic acid, was prepared as described elsewhere.[38] $NaCF_3SO_3$ was prepared by neutralization of (trifluoromethylsulfonic acid (Fluka) with NaOH, recrystallized from aqueous solution, and dried at 130 °C/10^{-3} Pa. $LiN(CF_3SO_2)_2$ (Fluorad HQ 115 from 3M) was dried at 130 °C/10^{-3} Pa. Propylene carbonate (PC, Burdick&Johnson), ethylene carbonate (EC, Fluka), and 1,2-dimethoxyethane (DME, Fluka) were dried over a molecular sieve (Union Carbide 4A). A 1 M solution of $LiN(CF_3SO_2)_2$ + EC/DME contained about 15 ppm of water (Karl-Fischer titration; Metrohm, model 684 KF coulometer). A 0.5 M solution of $NaCF_3SO_3$ was finally dried with Na+K alloy (35% Na);[39] the water content was <1 ppm.

Growth of Anatase Crystals. The crystals were grown in evacuated (10^{-3} Pa) quartz glass ampules containing typically 1 g of TiO_2 powder, 6 mg/mL of $TeCl_4$ (referred to the ampule volume), and 0.2−0.5 mol % of Al_2O_3 (referred to the TiO_2 mass). The ampule was introduced into a 3-zone semitransparent gold-coated furnace, which enabled a visual inspection of the crystal growth. The highest temperature allowing the growth of anatase was 670−680 °C (in narrow ampules 700 °C), and the optimum pressure of $TeCl_4$ was about 350 kPa. Frequently, anatase and rutile crystals were obtained together. Rutile was in the form of yellowish crystalline aggregates, strongly attached to the ampule walls. The anatase crystals were practically colorless transparent bipyramids with well-developed and highly reflecting (101) faces. They could easily be removed from the quartz walls. High-quality anatase crystals of about 10 mm^3 (36 mg) were obtained during 5−12 weeks of growth. Chemical analysis by ICP (see below) gave 0.22−0.53% Al, 150−240 ppm Nb, 170−260 ppm V, 90−140 ppm Zr, and 12−14 ppm La for crystals from different batches. The anatase phase was identified by X-ray diffraction of powdered crystals using a Guinier-deWolff (Nonius) camera and Cu Kα radiation.

(18) Tang, H.; Berger, H.; Schmid, P. E.; Lévy, F.; Burri, G. *Solid State Commun.* **1993**, *87*, 847.
(19) Forro, L.; Chauvet, O.; Emin, D.; Zuppiroli, L.; Berger, H.; Lévy, F. *J. Appl. Phys.* **1994**, *75*, 633.
(20) Chauvet, O.; Forro, L.; Kos, I.; Mijak, M. *Solid State Commun.* **1995**, *93*, 667.
(21) Sanjinés, R.; Tang, H.; Berger, H.; Gozzo, F.; Margaritonda, G.; Lévy, F. *J. Appl. Phys.* **1994**, *75*, 2945.
(22) Finklea, H. O. In *Semiconductor Electrodes, Studies in Physical and Theoretical Chemistry;* Finklea, H. O., Ed.; Elsevier: Amsterdam, 1988; Vol. 55, pp 43−145.
(23) Fujishima, A.; Honda, K. *Nature* **1972**, *238*, 37.
(24) (a) O'Regan, B.; Grätzel, M. *Nature* **1991,** *353*, 737. (b) Hagfeldt, A.; Grätzel, M. *Chem. Rev.* **1995,** *95*, 49.
(25) (a) Zachau-Christiansen, B.; West, K.; Jacobsen, T.; Skaarup, S. *Solid State Ionics* **1992,** *53*−56, 364. (b) Kawamura, H.; Muranushi, Y.; Miura, T.; Kishi, T. *Denki Kagaku* **1991**, *59*, 766.
(26) Zachau-Christiansen, B.; West, K.; Jacobsen, T.; Atlung, S. *Solid State Ionics* **1988,** *28*−30, 1176.
(27) Murphy, D. W.; Cava, R. J.; Zahurak, S. M.; Santoro, A. *Solid State Ionics* **1983**, *9&10*, 413.
(28) Bonino, F.; Busani, L.; Lazzari, M.; Manstretta, M.; Rivolta, B.; Scrosatti, B. *J. Power Sources* **1981**, *6*, 261.
(29) Ohzuku,T.; Takehara, Z.; Yoshizawa, S. *Electrochim. Acta* **1979**, *24* 219.
(30) Murphy, D. W.; Christensen, P. A.; Carides, J. N.; di Salvo, F. J. In *Fast Ion Transport in Solids;* Vashista, P., Mundy, J. N., Shenoy, G. K., Eds.; N. Holland: Amsterdam, 1979; p 137.
(31) Macklin, W. J.; Neat, R. J. *Solid State Ionics* **1992**, *53*−56, 694.
(32) Johnson, O. W. *Phys. Rev. A* **1964**, *136*, 284.
(33) Kanamura, K.; Yuasa, K.; Takehara, Z. *J. Power Sources* **1987**, *20*, 127.
(34) Cantão, M. P.; Cisneros, J. I.; Torresi, R. M. *J. Phys. Chem.* **1994**, *98*, 4865.
(35) Ohzuku, T.; Kodama, T. *J. Power Sources* **1985**, *14*, 153.
(36) Cava, R. J.; Murphy, D. W.; Zahurak, S.; Santoro, S.; Roth, R. S. *J. Solid State. Chem.* **1984**, *53*, 64.
(37) Voinov, M. Proceedings of the 158th Meeting of the Electrochemical Society, Hollywood, CA, 1980; Electrochemical Society, Pennington, NJ, p 74.
(38) Nazeeruddin, M. K.; Kay, A.; Rodicio I.; Humphry-Baker, R.; Müller, E.; Liska P.; Vlachopoulos, N.; Grätzel, M. *J. Am. Chem. Soc.* **1993**, *115*, 6382.
(39) Kavan, L.; Kratochvilová, K.; Grätzel, M. *J. Electroanal. Chem.* **1995**, *394*, 93.

Crystal Pretreatment and Mounting. Electrodes were prepared from anatase crystals containing 0.22% Al. The crystals were doped by reduction in a H_2−Ar (5−8% H_2) mixture or pure H_2 at 500−600 °C. At these conditions no transformation to rutile was observed. Larger crystals (up to 36 mg) were uniformly doped only at 600 °C in pure hydrogen after 24 h. The course of gradual doping manifested itself by color changes to ruby red, blue, and finally almost black. The process was reversible, i.e. a complete bleaching occurred in O_2 at 550−600 °C. This contrasts the results obtained by Lévy et al.,[21] who observed a color change of their highly doped crystals from blue to dark green in oxygen under similar conditions. The doped black crystal was contacted by a Ga−In alloy to a Cu wire. The wire and contact were isolated by a Torr-Seal epoxy (Varian) and protected by an E 43 silicone rubber seal (Wacker Chemie). Three different electrodes were prepared for parallel experiments. In all cases, only the (101) faces were exposed. Their areas were 0.90, 1.24, and 4.27 mm^2, respectively, as measured by optical microscopy. The crystal orientation was confirmed by X-ray diffraction (Laue camera). For comparison, also rutile (001) electrode (Crystal GmbH, Germany) was used. The methods of n-doping, contacting, and mounting were the same as for anatase.

Methods. Trace analysis was performed by inductively-coupled plasma emission spectrosocpy using a Perkin-Elmer ICP 1000 apparatus. The sample crystals were finely ground in an agate mortar, washed with 1 M HNO_3, and dissolved in a mixture of boiling 40% HF + 65% HNO_3 (7:1 by volume). The solution was then treated by 2.5 mL of 96% H_2SO_4 and evaporated almost to dryness; the last step was repeated twice. All acids were from Merck (Suprapur grade). Electrochemical measurements were carried out in conventional three-electrode cells using a PAR EG&G model 273 A apparatus. For photoelectrochemical experiments, the cell was equipped with a quartz glass window, and the working electrode was illuminated by an Oriel 450-W high-pressure xenon lamp in conjunction with a Bausch & Lomb high-intensity monochromator. The reciprocal dispersion was 6.4 nm (slit width 1 mm) and the monochromatic light intensity was about 0.2−7.5 W/m^2 at λ = 280−750 nm (YSI Kettering Model 65 A radiometer). The distance between the cell window and the electrode surface was about 5 mm. The Mott−Schottky plots were measured using an Autolab electrochemical unit (Ecochemie, The Netherlands). Simultaneous generation of several frequencies superimposed on the excitation signal was employed to detect dispersion effects. The measured signals were deconvoluted with a fast Fourier transform routine supplied with the Autolab software. Experiments with aprotic electrolyte solutions were performed in an argon-filled glovebox (1−5 ppm H_2O, 1−10 ppm O_2). In this case, the reference and auxiliary electrodes were both Li or Na, depending on the electrolyte cation. In aqueous medium, the saturated calomel electrode (SCE) served as the reference electrode and Pt as the counter electrode.

3. Results and Discussion

Interfacial Capacitance. Figure 1 displays the Mott−Schottky plots obtained with the anatase single-crystal electrode. The plots fit the equation

$$C^{-2} = 2(U - U_{fb} - kT/e)/e\epsilon_0\epsilon_r N \qquad (2)$$

(C is the capacitance, U is the electrode potential, U_{fb} is the flatband potential, k is the Boltzmann constant, T is the temperature, e is the electron charge, ϵ_0 is the permittivity of the vacuum, ϵ_r is the dielectric constant, and N is the donor density). Assuming the dielectric constant of anatase ϵ_r = 31,[40,41] the donor density N equals (0.4−0.8) × 10^{19} cm^{-3} at 100−1000 Hz (Figure 1). Analogous plots for rutile (not shown) give 1−2 × 10^{19} cm^{-3} assuming ϵ_r = 173.[22]

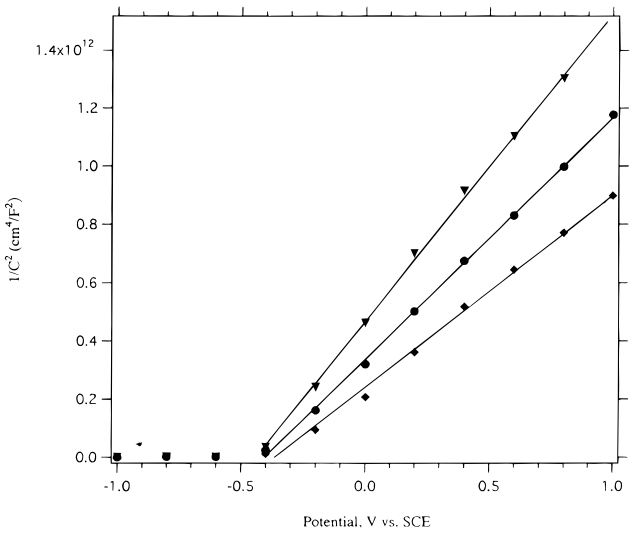

Figure 1. Mott−Schottky plots of the anatase single-crystal electrode in 1 M H_2SO_4. Frequencies: 100 (diamonds), 500 (circles), 1000 Hz (triangles).

The flatband potentials fit the equation

$$U_{fb} = U_o - 0.06\text{pH}[V, \text{vs SCE}] \qquad (3)$$

where U_o was found to be −0.20 V for rutile and −0.4 V for anatase (Figure 1). For polycrystalline anatase, similar U_o values have been reported.[42]

Since the flatband potential in aqueous electrolyte solutions roughly matches the potential of a hydrogen electrode, capacitive effects in the accumulation regime can be studied only in aprotic media. For instance, solutions of (trifluoromethyl)sulfonates in dry propylene carbonate offer a rather broad interval of potentials negative to flatband, where the spurious faradic reactions can be neglected.[39] The formation of an accumulation layer can be conveniently followed by cyclic voltammetry. The steady-state voltammetric current density (i) at the given potential (U) and scan rate (υ) is related to the interfacial capacitance (C) as follows:

$$i = dq/dt = C\,dU/dt = C\upsilon \qquad (4)$$

(q is the accumulated charge density).

Figures 2 and 3 show cyclic voltammograms of rutile and anatase electrodes, respectively, in 1 M $NaCF_3SO_3$ + PC at various scan rates between 20 and 500 mV/s. The total integrated anodic voltammetric charge at v = 500−0.1 mV/s equals 40−110 $\mu C/cm^2$ for rutile and 15−60 $\mu C/cm^2$ for anatase. The insets display, according to eq 3, the interfacial capacitance as a function of potential. Similar values were reported for single-crystal rutile[43] and polycrystalline anatase[39] in aprotic media. The interfacial capacitance and flatband potential are, however, controlled by surface OH groups, which can be removed only by heat treatment above 400 °C.[39] This is technically impossible for our epoxy-mounted crystals, hence, we can make only a qualitative comparison of Figures 2 and 3. Anatase (Figure 3) shows a negative shift of the potential onset for the cathodic capacitive current. This potential is close to the flatband potential, i.e. a negative shift in flatband potentials of anatase vs rutile is apparent also in aprotic medium (cf. eq 2). Additionally, rutile exhibits a less smooth voltammogram around the flatband potential. This effect is typical for polycrystalline electrodes and can be attributed to the charging/discharging of surface states.[39] On rutile, the surface states are introduced through mechanical defects, because commercial

(40) Tang, H.; Prasad, K.; Sanjinés, P. E.; Schmid, P. E.; Lévy, F. *J. Appl. Phys.* **1994**, *75*, 2042.
(41) Roberts, S. *Phys. Rev.* **1949**, *76*, 1215.
(42) Rothenberger, G.; Fitzmaurice, D.; Grätzel, M. *J. Phys. Chem.* **1992**, *96*, 5983.
(43) Schumacher, R.; Teschner, D. M.; Heinzel, A. B. *Ber. Bunsenges. Phys. Chem.* **1982**, *86*, 1153.

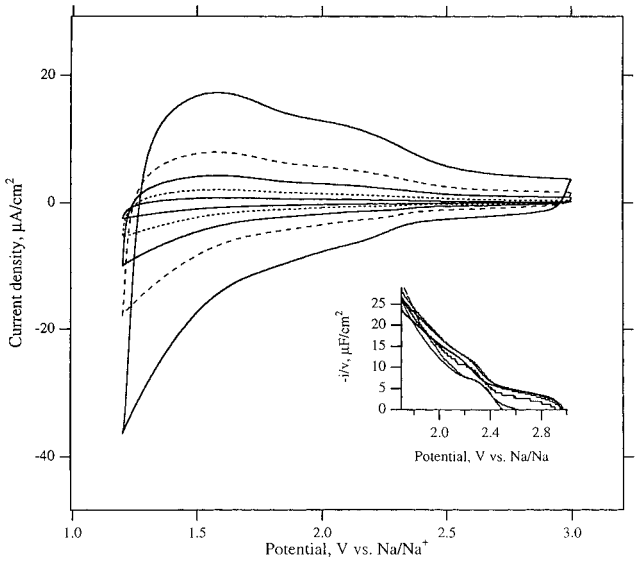

Figure 2. Cyclic voltammograms of the rutile single-crystal electrode in 0.5 M $NaCF_3SO_3$ + PC at scan rates v = 500, 200, 100, 50, and 20 mV/s. The inset shows $-i/\upsilon$ vs potential for the negative sweeps at $10 < \upsilon < 1000$ mV/s.

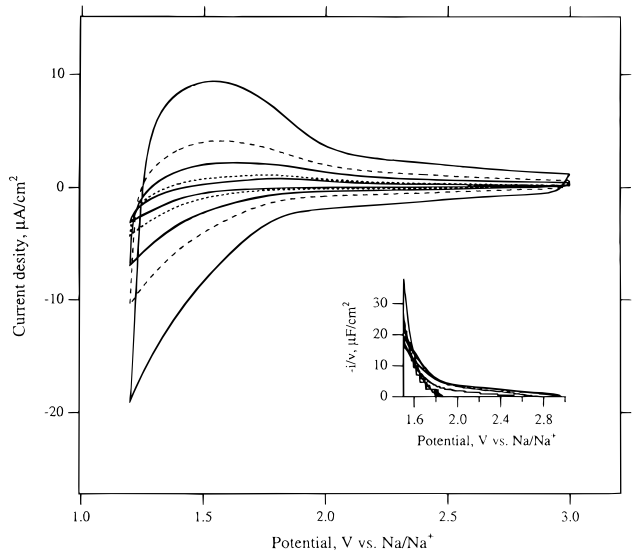

Figure 3. Cyclic voltammograms of the anatase single-crystal electrode in 0.5 M $NaCF_3SO_3$ + PC at scan rates v = 500, 200, 100, 50, and 20 mV/s. The inset shows $-i/\upsilon$ vs potential for the negative sweeps at $10 < \upsilon < 1000$ mV/s.

rutile chips (see the Experimental Section) are sliced from boules grown by the Verneuil method and polished. Flame fusion (Verneuil) grown rutile has typically $>10^6$ dislocations per cm^2 and grain boundaries (mosaic) up to 1°. In contrast, faceted anatas grown quasi-isothermally from the gas phase has a high structural perfection, as is evident from the surface morpholgy of the facets. Consequently, no voltammetric peaks of surface states are apparent for the latter crystals in Figure 3.

Photoelectrochemical Oxidation of Water. Figure 4 displays the photocurrent action spectrum in aqueous 1 M Na_2SO_4 solution (pH 6.4) where the incident photon-to-electron conversion efficiency (η) is plotted as a function of excitation wavelength.

$$\eta = ihc/\lambda Pe \tag{5}$$

(i is the photocurrent density, h is Planck's constant, c is the velocity of light, λ is the wavelength, and P is the light intensity (in W/m^2)). P is the incident light power, determined in front

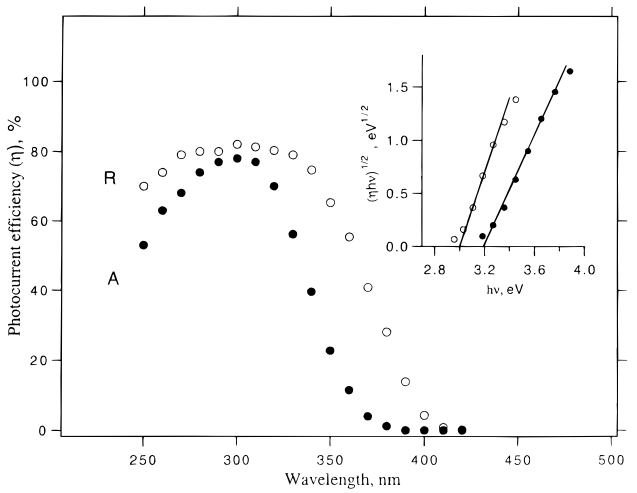

Figure 4. Photocurrent action spectrum of single-crystal rutile (R, open circles) and anatase (A, solid circles) in aqueous 1 M Na_2SO_4 (pH 6.4). The electrode potential was 1.0 V vs SCE. Inset: Data replotted for the estimation of band gap; anatase = solid circles, rutile = open circles.

of the window, which is not corrected for absorption and reflection losses in the window, electrolyte solution, and electrode. These losses cannot be determined precisely, but assuming that they are roughly 10−20%,[44] both our electrodes show a quantum yield of photocurrent close to unity at 300 nm.

Neglecting the e^-h^+ recombination in the space charge layer (width W), and supposing that the penetration depth of light ($1/\alpha$; α is optical absorption coefficient) is much higher than W and than the hole diffusion length (L), the efficiency η can be correlated to the photon energy by the equation

$$\eta h\nu/e = A(L + W)(h\nu - E_g)^m \tag{6}$$

where E_g is the band-gap energy while the exponent m equals $^1/_2$ for a direct and 2 for an indirect electronic transition.

The inset in Figure 4 shows that eq 5 with $m = 2$ is closely followed in a range of photon energies close to the absorption threshold indicating that the optical transition near the band gap is indirect. From the intercepts of the straight lines with the abscissa, the band gap energies for anatase and rutile are derived as 3.2 and 3.0 eV, respectively. Similar values were derived previously from optical measurements on rutile[22] and anatase[18] single crystals, and on polycrystalline materials,[40,45] although in ref 45 the anatase transition at 3.2 eV was reported to be a direct one.

Figure 5 shows a comparison of the photocurrent voltage curves obtained with rutile and anatase under illumination with white light from the Oriel 450-W Xe lamp. Due to the higher band gap the plateau currrent for anatase is about 3 times lower than that for rutile. In addition, the onset of the anodic photocurrent of the former is displaced negatively by 0.25 V with respect to the latter. This confirms that the increased band gap of anatase affects only the position of the conduction−and not that of the valence band edge. While the flat-band potential of rutile is slightly more positive than that of the standard hydrogen electrode, the flat-band potential of anatase is clearly negative of it. Thus, the reduction of water to H_2 by photogenerated conduction band electrons proceeds spontaneously with anatase, but not with rutile. This is clearly apparent from Figure 5 where a significant photocurrent is discernible at the reversible

(44) Kavan, L.; Grätzel, M. *Electrochim. Acta* **1995**, *40*, 643.
(45) Minoura, H.; Nasu, M.; Takahashi, Y. *Ber. Bunsenges. Phys. Chem.* **1985**, *89*, 1064.

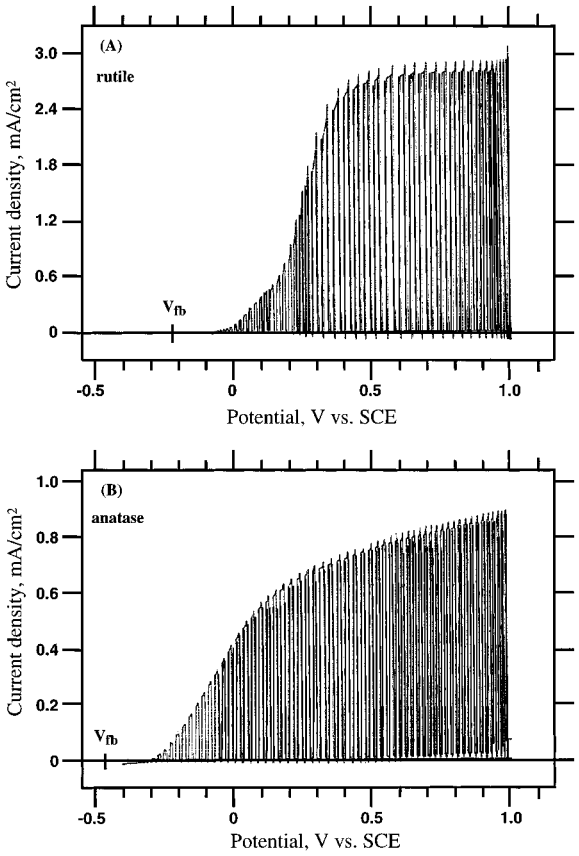

Figure 5. Photocurrent−voltage curve of single-crystal rutile (A) and anatase (B). Excitiation with the full output of the 450-W Xe lamp which was chopped to obtain the dark current at each applied potential. The electrolyte was 0.5 M aqueous H_2SO_4.

hydrogen electrode potential (−0.24 V vs SCE) for anatase while no photocurrent is detectable at this voltage for the rutile modification. The potential of photogenerated holes is identical for both polymorphs and well above the potential of O_2 evolution. Therefore, *anatase is the only known modification of TiO_2, on which the complete photoelectrolysis of water can take place without external bias.*

The photooxidation of water on TiO_2 initially produces surface-bound intermediates, presumably peroxides,[46] whose formation can be monitored by cyclic voltammetry. The presence of peroxides manifests itself by an irreversible cathodic peak appearing close to the flat-band potential upon sweeping the potential negatively in the dark. It was previously reported that the surface peroxides are formed only on anatase, not on rutile.[46] However, we have observed the cathodic current peak characteristic for the reduction of these photogenerated intermediates with anatase as well as rutile single-crystal electrodes, indicating that surface peroxide formation takes place on both materials. Photogeneration of reducible species on single-crystal TiO_2 also has been mentioned by other authors although the crystal structure is often not specified.[47]

Sensitized Photoinjection of Electrons. Sensitization of single-crystal electrodes was performed by adsorption of *cis*-$RuL_2(SCN)_2$ according to a previously described procedure.[38] Typically, the electrodes were dipped for 2−12 h in a 3×10^{-4} M solution of the ruthenium complex in ethanol at room

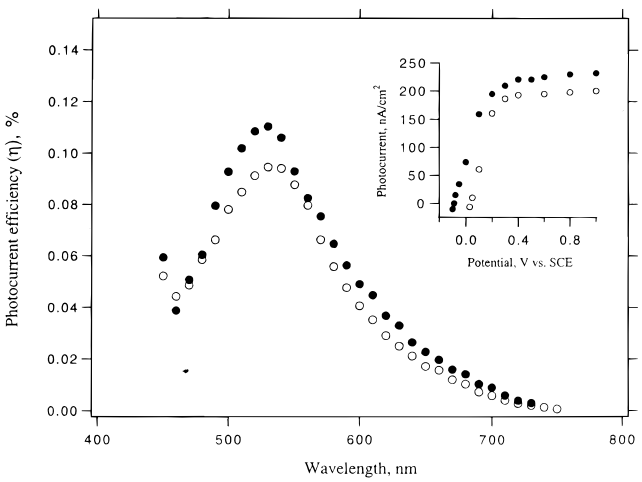

Figure 6. Photocurrent action spectrum of single-crystal rutile (open points) and anatase (full points) sensitized with *cis*-Ru[$L_2(SCN)_2$], L = 2,2′-bipyridyl-4,4′-dicarboxylic acid). Electrolyte solution: aqueous 0.3 M LiI, pH 2.0. The electrode potential was 1.0 V vs SCE. Inset: Photocurrent-Potential curve at $\lambda = 500$ nm.

temperature. Figure 6 displays the action spectrum obtained with aqueous 0.3 M LiI electrolyte at pH 2.0. The photocurrent efficiency is again defined by eq 4, i.e. it is not corrected for absorption and reflection losses. The efficiencies at $\lambda < 450$ nm (not shown) are lowered by the optical absorption of the electrolyte solution (I_3^- species formed by oxidation of iodide). The inset shows the photocurrent−potential curve for the same system under illumination with 500-nm light. The potential for the anodic photocurrent onset is 0.1 V more negative for anatase as compared to rutile, in qualitative agreement with the difference in the flat-band potential of the two polymorphs.

A cathodic photocurrent was observed for both the anatase and rutile single-crystal electrodes at potentials negative of the intercepts of the photocurrent curves with the abscissa in Figure 6. A similar phenomenon has been reported first by Calvin et al.[48] for TiO_2 sensitized with rose bengal. Goodenough et al.[49] have found an analogous effect for $Ru(bpy)_3^{2+}$−TiO_2 at potentials ca. 0.4−0.5 V positive to U_{fb}. The effect has been explained in terms of energy transfer from the photoexcited dye to the filled electronic surface states of TiO_2 and a modulation of the background dark current.[22] Polycrystalline anatase sensitized by various Ru(II) bipyridine complexes exhibits an onset of anodic photocurrent at potentials 0.23−0.38 V positive to U_{fb} defined by eq 2 depending on light intensity.[50,51] No comparable data for rutile are available. The shift of the potential for anodic photocurrent onset observed here for single-crystal anatase is in the same range.

Assuming that the quantum yield for charge injection from the excited sensitizer in to the TiO_2 is one and that the injected electrons are collected with unit efficiency and neglecting optical losses by absorption and reflection, the photon to current conversion efficiency equals the light harvesting yield:

$$\eta = 1 - 10^{-\epsilon\Gamma} \qquad (7)$$

where ϵ is the extinction coefficient of the sensitizer, and Γ is its surface coverage. The surface coverage Γ was determined

(46) Augustynski, J. *Electrochim. Acta* **1993**, *38*, 43.
(47) (a) Sprünken, H. R.; Schumacher, R.; Schindler, R. N. *Faraday Discuss. Chem. Soc.* **1980**, *70*, 55. (b) Finklea, H. O.; Murray, R. W. *J. Phys. Chem.* **1979**, *83*, 353. (c) Wilson, R. H. *J. Electrochem. Soc.* **1980**, *127*, 228. (d) Nakato, Y.; Tsumura, A.; Tsubomura, H. *J. Phys. Chem.* **1983**, 87, 2402.
(48) Spitler, M. T.; Calvin, M. *J. Chem. Phys.* **1977**, *66*, 4294.
(49) Hamnett, A.; Dare-Edwards, M. P.; Wright, R. D.; Seddon, K. R.; Goodenough, J. B. *J. Phys. Chem.* **1979**, *83*, 3280.
(50) O'Regan, B.; Moser, J.; Anderson, M.; Grätzel, M. *J. Phys. Chem.* **1990**, *94*, 8720.
(51) (a) Liska P.; Vlachopoulos, N.; Nazeeruddin, M.; Comte, P.; Grätzel, M. *J. Am. Chem. Soc.* **1988**, *110*, 3686. (b). Vlachopoulos, N.; Liska P.; Augustynski, J.; Grätzel, M. *J. Am. Chem. Soc.* **1988**, *110*, 1216.

for $Ru[L_2(SCN)_2]$ on rutile (001) as $(9.2 \pm 0.3) \times 10^{-11}$ mol/cm^2, i.e. 1.8 ± 0.5 nm^2/molecule.[52] A monolayer of rose bengal or $RuL(bpy)_2$ on rutile (001) corresponds to 0.75 nm^2/molecule[48] or 1.7 nm^2/molecule,[53] respectively. Similar values were reported also for other Ru(II) bipyridine complexes adsorbed on polycrystalline anatase.[54,55] No data for single-crystal anatase are available.

Using $\Gamma = 9.2 \times 10^{-11}$ mol/cm^2 and $\epsilon = 1.27 \times 10^7$ cm^2/mol the incident photon-to-current conversion efficiency at 530 nm is predicted by eq 6 to be 0.27%. The experimental values for both TiO_2 polymorphs in Figure 5 are almost three times smaller, i.e. 0.1%. The difference can hardly be attributed to optical losses alone. For the experimental setup employed, these are estimated to be ca. 20%[24,38,44] in agreement with the UV excitation results in Figure 4. Our data rather point at lower charge injection and/or collection efficiencies at the single-crystal electrodes as compared to nanocrystalline anatase films. The latter convert practically all the absorbed light into electric current when sensitized with *cis*-$RuL_2(SCN)_2$.[38] This observation is astonishing given the disordered structure of the nanocrystalline layers and the absence of a space charge field in the mesoscopic TiO_2 particles. One would in fact have expected the opposite behavior since the electric potential gradient in the depletion layer of the TiO_2 single crystals favors both the charge separation and collection process. The band bending at the surface of the single-crystal electrode is much more pronounced than in the case of the mesoporous anatase film due to the formation of a depletion layer at the semiconductor−electrolyte contact. From the flat-band potential of −0.5 V vs SCE at pH 2 and the applied potential of 1 V vs SCE (as in Figure 6), the reverse bias is 1.5 V. This voltage is expected to drop within the space charge region of the single crystal while the potential drop in a nanocrystalline particle is at best a few millivolts.[50]

The precise origin of this striking difference in the sensitization behavior of mesoscopic particle films and single crystals of anatase remains to be determined. One can exclude structure-specific effects arising from the adsorption of the sensitizer to different types of lattice planes since the surface of the anatase nanoparticles consists mainly of (101) faces,[56] i.e. the same type that is exposed in the case of the single-crystal electrode. A rational may be provided by the widely different doping levels of the two materials. While the nanocrystalline films are virtually intrinsic ($N < 10^{17}$ cm^{-3}),[50] the donor densities in the single crystals are rather high, i.e. of the order of 10^{19} cm^{-3}. The higher conduction band electron concentration may enhance electron recapture by the charge-transfer sensitizer, or afford energy-transfer quenching of the excited dye. Both processes decrease the photon-to-current conversion efficiency. However, since the measurements in Figure 5 were carried out under a reverse bias of 1.5 V, the surface-electron concentration is close to that of intrinsic anatase. Energy transfer quenching is unlikely to occur under these conditions. The effect has been extensively studied in the context of electroluminescent ions adsorbed on semiconductor surfaces[57] where it was detected only at potentials close to flat-band condition or under forward bias. This indicates that high surface-electron concentrations are required to render energy transfer quenching efficient. As to the likelihood of electron recapture by the oxidized dye, this could occur even under reverse bias via electron tunneling from the conduction band through the space charge layer to the adsorbed sensitizer. However, at 1.5 V reverse bias the width of the depletion layer in the anatase single crystal is rather large, i.e. about 33 nm, a distance too long to allow for electron tunneling to take place in the nano- to microsecond time domain decisive for the yield of interfacial charge separation. Note also that the photon-to current conversion yields are nearly independent of the applied potential over a large voltage range as shown in the inset of Figure 6. Hence, effects arising from the space-charge layer field which is present in the single crystal but absent in the mesosocopic film of anatase can not account for the difference in the photon-to-current conversion efficiencies observed between these two materials. Although further studies are required to unravel the reasons for this very intriguing difference, we note that the observation made recently by Parkinson et al.[58] on dye-sensitized single-crystal SnS_2 photoelectrodes may be closely related to our findings. These authors detected a large increase in the yield of electron flow per absorbed photon upon etching the surface indicating that roughening of the SnS_2 has a beneficial effect on the efficiency of light-induced charge separation. The striking conclusion which can be drawn from these findings is that dye adsorption on a perfectly smooth surface, such as the van der Waals plane of SnS_2, leads to lower photocurrent yields than in the case where the sensitizer is deposited on a roughened surface distinguished by structural imperfections and a porous morphology. This is definitely an unexpected result which points at the important role surface texture plays in controlling the performance of these types of injection solar cells.

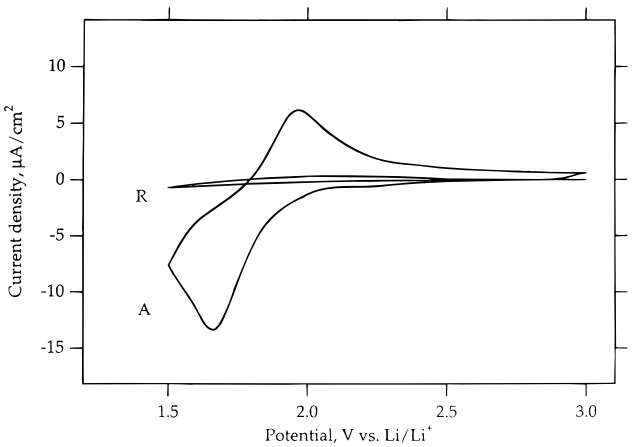

Figure 7. Cyclic voltammogram of single-crystal anatase (A) and rutile (R) in 1 M $LiN(CF_3SO_2)_2$ + EC/DME (1:1 by mass). the scan rate is 0.1 mV/s.

Lithium Insertion. Figure 7 shows cyclic voltammograms of the anatase and rutile electrodes in 1 M $LiN(CF_3SO_2)_2$ + EC/DME. The quasireversible insertion/extraction of Li^+ in anatase is clearly apparent, whereas rutile gives much weaker effects at the same conditions. Integration of the total anodic voltammetric charge in Figure 6 gives 1.86 mC/cm^2 for rutile, which is by one order of magnitude larger than the capacitive charge in electrolyte solution containing Na^+ (cf. Figure 2 and discussion above). It translates into an effective Li^+ insertion

(52) The measurement of Γ was carried out spectrophotometrically, while the optical absorbance (at $\lambda = 530$ nm) of ten monolayers of the dye on five stacked rutile wafers (10 × 10 × 1 mm) was recorded.[48] Better results were obtained if the dye was desorbed from the rutile wafers by 0.1 M NaOH, and the eluent analyzed spectrophotometrically at $\lambda = 309$ nm.

(53) Dare-Edwards, M. P.; Goodenough, J. B.; Hamnett, A.; Seddon, K. R.; Wright, R. D. *Trans. Faraday Soc.* **1980**, *70*, 285.

(54) Nazeeruddin, M. K.; Liska, P.; Moser, J.; Vlachopoulos, N.; Grätzel, M. *Helv. Chim. Acta* **1990**, *73*, 1788.

(55) Furlong, D. N.; Wells, D.; Sasse, W. H. F. *J. Phys. Chem.* **1986**, *90*, 1107.

(56) Shklover, V.; Comte, P.; Grätzel, M.; Nesper, R.; Hermann, R. *J. Mater. Chem.* Submitted for publication.

(57) Meulenkamp, E. A. Ph.D. Thesis, University of Utrecht, The Netherlands, 1993.

(58) Sharp, L.; Louder, D.; Parkinson, B. A. Proceedings of the 19th DOE Solution Photochemistry Research Conference, 1995.

distance of 7 nm assuming the product composition $Li_{0.5}TiO_2$. This value is comparable to the thickness of the accumulation layer on TiO_2.[34,42] The Li^+ insertion in rutile is strongly anisotropic (one-dimensional) *via* free channels along the *c* axis.[22,32] Nevertheless, only small amounts of Li^+ can be accommodated into the bulk crystal even in the ideal electrode orientation (001). This matches the conclusions of refs 26−30,59, but contrasts ref 31. A theoretical approach to rationalize the different behavior of rutile and anatase with respect to Li^+ intercalation has been made by Stashans et al.[59]

Facile lithium intercalation into mesoporous anatase films has been reported by severals groups,[60−63] and this effect has been exploited to realize an electrochromic device[61] and a new type of intercalation battery.[63]

The insertion channels in anatase run along the *a* axes.[22] Although our anatase electrode is not ideally oriented (the exposed face is (101)), the integrated anodic voltammetric charge is by one order of magnitude higher than that for rutile (Figure 6); it amounts to 26.4 mC/cm^2, which corresponds to the effective insertion distance of 113 nm (for $Li_{0.5}TiO_2$). The striking difference between rutile and anatase is difficult to understand. Zachau-Christiansen[26] and Ohzuku[29] have suggested a simple interpretation based on the more dense packing of the rutile lattice, i.e. the empty channels along the rutile *c* axis are, reportedly, too narrow to accommodate Li^+.

However, this statement is problematic for at least four reasons: (i) Li^+ diffuses rapidly through the rutile *c* channels, the diffusion coefficient, *D*, being of the order of 10^{-6} cm^2/s at room temperature.[32] (ii) The approximate radius of the *c* channels in rutile is 80 pm, which is even larger than the radius of the a channels in anatase (70 pm).[22] (iii) At 120 °C, rutile accommodates Li^+ reversibly up to $x = 0.5$, where *x* is the molar ratio of lithium-to-titanium ions, but anatase shows significantly worse performance.[31] (iv) Ruthenium dioxide (rutile structure) accommodates Li^+ perfectly ($x = 1.3$) despite having almost the same unit cell volume as TiO_2 (rutile).[30] An interpretation that the highly conducting RuO_2 provides more efficient screening of Coulombic repulsion between Li^+ ions[30] is not convincing. The conductivity of the doped TiO_2 single crystals equals

$$\sigma = eN\mu \tag{8}$$

(μ is the electron mobility, about 1 cm^2/(V·s) for rutile[22] and 10 cm^2/(V·s) for anatase[19]). Hence, the conductivity is significant, and similar for both our rutile and anatase crystals, i.e. 1−10 S/cm assuming $N = 10^{19}$ cm^{-3}.

In the light of these considerations the theoretical studies of Stashans et al.[59] using quantum chemical Hartree−Fock calculations provide at present the best rational for explaining the striking difference in the lithium intercalation behavior observed between rutile and anatase. According to their analysis, the ease of lithium insertion into anatase is related to the much smaller distortion of the bulk lattice as compared to rutile. Due to the presence of structural voids, the accommodation of Li into the former requires a much smaller lattice relaxation than that for the latter polymorph. In the case of the rutile (110) surface the interclation appeared to be mainly a surface effect.

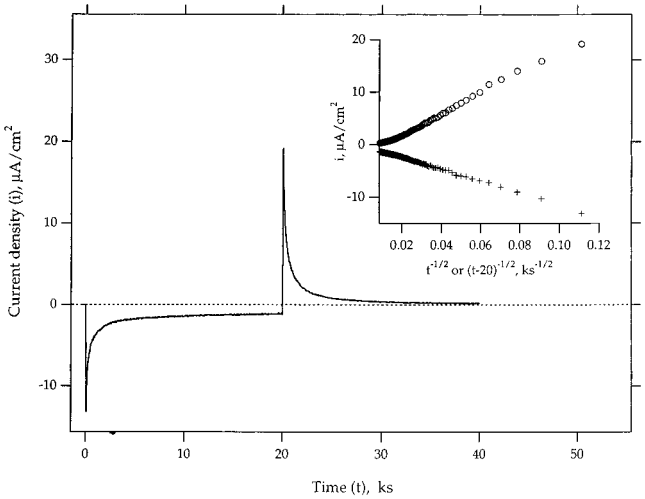

Figure 8. Chronopotentiometric plot of an anatase electrode in 1 M $LiN(CF_3SO_2)_2$ + EC/DME (1:1 by mass). The potential steps were 3.0 ± 1.5 V (at $t = 0$) and 1.5 ± 3.0 V (at t = 20 ks). The inset shows the same diagram in the coordinates: i vs $t^{-1/2}$ (first step) and i vs $(t - 20)^{-1/2}$ (second step).

Figure 8 displays chronoamperometric plots of anatase electrode into which Li^+ was inserted by applying a potential step from 3.0 to 1.5 V vs Li/Li^+, and subsequently extracted by using the opposite potential step, i.e. from 3.0 to 1.5 V vs Li/Li^+. The integrated anodic charge equals 92 mC/cm^2 which corresponds to the diffusion distance of 390 nm (assuming the composition $Li_{0.5}TiO_2$). The insertion/extraction follows formally the Cottrell equation:

$$i = FD^{1/2}c\pi^{-1/2}t^{-1/2} \tag{9}$$

(F is Faraday constant and c is the concentration of Li^+ in the solid). Assuming the composition of the subsurface layer to be $Li_{0.5}TiO_2$, the concentration c equals 24 mmol/cm^3. From the plots in Figure 8 the diffusion coefficient, *D*, is derived as 2×10^{-13} and 6×10^{-13} cm^2/s for the insertion and extraction, respectively. These values are comparable to those reported for polycrystalline materials.[33,34] The values obtained for the diffusion coefficients for Li-uptake and release indicate that the insertion process is three times slower than deintercalation. This could arise from the fact that Li-uptake is an activated process due to the lattice relaxation accompanying the accommodation of lithium in the host. Alternatively it may reflect the effect of solvent interaction with the lithium ions: during intercalation the solvent has to be removed from the lithium requiring an activation energy which is not necessary for the solvation of lithium during the deintercalation process.

4. Conclusions

Anatase single crystal containing 0.22% of Al and traces of V, Zr, Nb, and La has been studied for the first time as an electrode material. The crystal was grown by a chemical transport reaction employing $TeCl_4$. Electrodes were prepared from anatase crystals, doped by reduction with hydrogen. The exposed lattice plane was (101).

The flat-band potential of anatase (101) is shifted negatively by 0.2 V vs the flat-band potential of rutile (001). A Nernstian-type pH dependence of U_{fb} is apparent in aqueous electrolyte solutions. Interfacial capacitance, associated with the formation of accumulation layer in aprotic medium, indicates a lower contribution of surface states on anatase as compared to rutile. This is caused by higher perfection of the naturally grown (101) face of our anatase.

(59) Stashans, A.; Lunell, S.; Bergström, R.; Hagfeldt, A.; Lindquist, S. E. *Phys. Rev. B* **1996**, *53*, 1.
(60) Redmond, G.; Fitzmaurice, D. *J. Phys Chem.* **1993**, *97*, 1426.
(61) Hagfeldt, A.; Vlachopoulos, N.; Grätzel, M. *J. Electrochem. Soc.* **1994,** *142*, L82.
(62) Lion, L. A.; Hupp, J. T. *J. Phys. Chem.* **1995,** *99*, 15718.
(63) Huang, S. Y.; Kavan, L.; Exnar, I.; Grätzel, M. *J. Electrochem. Soc*. **1995**, *142*, L142.

Photoelectrochemical oxidation of water proceeds on both rutile and anatase electrodes with incident photon-to-current efficiencies close to unity at $\lambda \cup 300$ nm. The products (presumably surface peroxides) are electrochemically reducible in the dark. Analysis of the photocurrent action spectrum gives the indirect band gap of anatase and rutile as 3.2 and 3.0 eV, respectively. From the comparison of U_{fb} and E_g, it follows that anatase (101) and rutile (001) electrodes differ mainly in the position of the conduction band edge. The complete photoelectrolysis of water to H_2 and O_2 is thermodynamically possible on anatase only.

Photosensitized electron injection from adsorbed *cis*-Ru[L_2-$(SCN)_2$] into the TiO_2 conduction band proceeds with comparable efficiencies on both anatase and rutile electrodes. However, the yield of photocurrent flow per absorbed photon is about 3 times smaller for the single crystals as compared to nanocrystalline anatase films. The detailed reasons for this striking and unexpected effect of the surface texture on the efficiency of light induced charge separation remain to be unraveled.

Anatase (101) is considerably more active for electrochemical insertion of Li^+ than rutile (001). This is surprising, since the insertion channels in rutile are in the ideal orientation toward the electrode surface. The anatase (101) face accommodates 26−92 mC/cm^2 of Li^+ in different potentiodynamic experiments lasting about 4−6 h. The diffusion coefficients for Li^+ insertion/extraction were estimated from chronoamperometric plots as 2×10^{-13} and 6×10^{-13} cm^2/s, respectively.

Acknowledgment. We wish to thank the Institute for Applied Photovoltaics (INAP), Gelsenkirchen, Germany, for financial assistance. Dr. Didier Perret (University of Lausanne) has contributed with ICP analyses.

JA954172L